Research Article

Nano Research
2022, 15(6): 5510–5516

ISSN 1998-0124 CN 11-5974/O4
https://doi.org/10.1007/s12274-022-4190-0

Highly sensitive, scalable, and rapid SARS-CoV-2 biosensor based on In_2O_3 nanoribbon transistors and phosphatase

Mingrui Chen[1,§], Dingzhou Cui[2,§], Zhiyuan Zhao[1], Di Kang[6], Zhen Li[3], Shahad Albawardi[4], Shahla Alsageer[4], Faisal Alamri[4], Abrar Alhazmi[4], Moh. R. Amer[4,5] (✉), and Chongwu Zhou[1,2] (✉)

[1] *Mork Family Department of Chemical Engineering and Materials Science, University of Southern California, Los Angeles, California 90089, USA*
[2] *Ming Hsieh Department of Electrical Engineering, University of Southern California, Los Angeles, California 90089, USA*
[3] *Department of Physics and Astronomy, University of Southern California, Los Angeles, California 90089, USA*
[4] *Center of Excellence for Green Nanotechnologies, King Abdulaziz City for Science and Technology, Riyadh, Saudi Arabia*
[5] *Department of Electrical Engineering, 420 Westwood Plaza, 5412 Boelter Hall, University of California, Los Angeles, Los Angeles, California 90095, USA*
[6] *eDNA Biotech, Pasadena, California 91107, USA*
[§] *Mingrui Chen and Dingzhou Cui contributed equally to this work.*

Received: 24 November 2021 / **Revised:** 24 January 2022 / **Accepted:** 25 January 2022

ABSTRACT

Developing convenient and accurate SARS-CoV-2 antigen test and serology test is crucial in curbing the global COVID-19 pandemic. In this work, we report an improved indium oxide (In_2O_3) nanoribbon field-effect transistor (FET) biosensor platform detecting both SARS-CoV-2 antigen and antibody. Our FET biosensors, which were fabricated using a scalable and cost-efficient lithography-free process utilizing shadow masks, consist of an In_2O_3 channel and a newly developed stable enzyme reporter. During the biosensing process, the phosphatase enzymatic reaction generated pH change of the solution, which was then detected and converted to electrical signal by our In_2O_3 FETs. The biosensors applied phosphatase as enzyme reporter, which has a much better stability than the widely used urease in FET based biosensors. As proof-of-principle studies, we demonstrate the detection of SARS-CoV-2 spike protein in both phosphate-buffered saline (PBS) buffer and universal transport medium (UTM) (limit of detection [LoD]: 100 fg/mL). Following the SARS-CoV-2 antigen tests, we developed and characterized additional sensors aimed at SARS-CoV-2 IgG antibodies, which is important to trace past infection and vaccination. Our spike protein IgG antibody tests exhibit excellent detection limits in both PBS and human whole blood ((LoD): 1 pg/mL). Our biosensors display similar detection performance in different mediums, demonstrating that our biosensor approach is not limited by Debye screening from salts and can selectively detect biomarkers in physiological fluids. The newly selected enzyme for our platform performs much better performance and longer shelf life which will lead our biosensor platform to be capable for real clinical diagnosis usage.

KEYWORDS

biosensor, indium oxide transistor, phosphatase, SARS-CoV-2 spike protein, SARS-CoV-2 spike IgG antibody

1 Introduction

On the 11th of March 2020 the World Health Organization (WHO) declared Coronavirus disease 2019 (COVID-19) outbreak, caused by the severe acute respiratory syndrome coronavirus (SARS-CoV-2), as a pandemic [1]. SARS-CoV-2 can cause severe respiratory distress, and as of November 2021, cumulative number of infected people is over 250 million, resulting in over 5 million death all over the world [2, 3]. Owing to the high infectivity of the virus and lack of specific treatments against it, early diagnosis of COVID-19 is essential in pandemic prevention and control, which mandates a highly sensitive and yet more scalable, cost-efficient, and rapid detection method of SARS-CoV-2, particularly for developing countries carrying a heavy economic burden caused by COVID-19 pandemic [4].

SARS-CoV-2 mainly contains 4 types of proteins: spike(S), membrane(M), nucleocapsid(N), and envelop(E) proteins (Fig. 1(a)). Among these proteins, the S protein is on the viral envelope and its S1 subunit is the outermost component of the virus. During SARS-CoV-2 infection, S1 proteins recognize and bind with the cellular receptor on the surface of the target cells, facilitating the virus particles to enter the target cells and triggering the infection [5–8]. Therefore, S1 protein is an important target for SARS-CoV-2 diagnostic detection. Moreover, detecting S1 protein specific antibody in human blood is also important for COVID-19 diagnosis in terms of determining previous viral exposure and immunity status. Antibody tests (also known as serology test) can be nearly 100% accurate for blood samples collected 20 days after infection or the onset of symptoms [9–11]. In this work, we developed a versatile electronic biosensing platform detecting both SARS-CoV-2 S1 protein and S1 protein IgG antibody, whose detection target can be easily switched between the two biomarkers.

Address correspondence to Moh. R. Amer, mamer@seas.ucla.edu; Chongwu Zhou, chongwuz@usc.edu

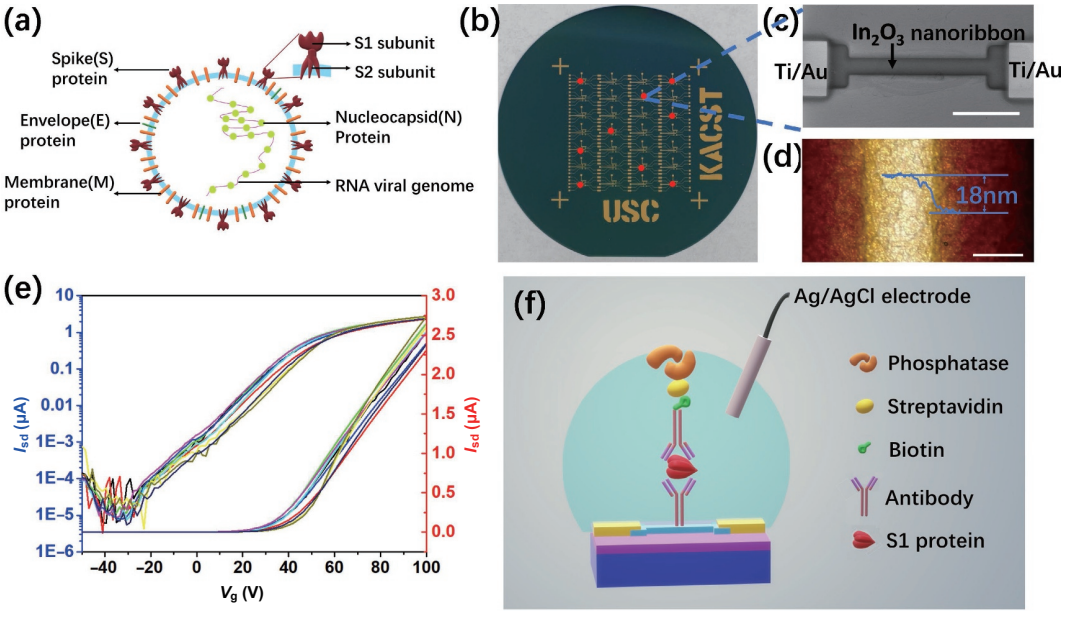

Figure 1 (a) Schematic structure of SARS-CoV-2. (b) Optical image of a 3-inch wafer with an In_2O_3 nanoribbon biosensors. (c) Scanning electron microscope image of the channel region of one device (L = 500 μm, W = 25 μm). The scale bar is 200 μm. (d) Atomic force microscopy image of a ~18 nm thick In_2O_3 nanoribbon. The scale bar is 20 μm. (e) Drain current versus back gate voltage of nine In_2O_3 nanoribbon FET devices with locations labelled in (b) by red dots, with drain voltage fixed at 1 V, plotted in linear and logarithmic scale. (f) Schematic illustration of the electronic biosensing setup for S1 protein detection.

Thus far, based on previously established laboratory protocols, diagnosis of COVID-19 depends mainly on nucleic acid amplification tests (NAATs), specifically real-time reverse transcription-polymerase chain reaction (RT-PCR) [12–14]. Although this method is sensitive and shows good specificity for COVID-19 detection, this technique has a long processing time (usually 4–5 h) and depends on advanced instruments, expensive reagents, and skilled technicians.

Among recent advances in rapid screening methods, field-effect transistor (FET)-based biosensors have many advantages such as small size, real-time detection, high-sensitivity, and capability for integrated multiplexing [15–20]. Seo et al. reported graphene-based FET biosensors for spike protein of SARS-CoV-2 [21], and Shao et al. demonstrated single-walled carbon nanotube (SWCNT)-based FETs to probe spike and nucleocapsid proteins of SARS-CoV-2 [22]. As it is widely known, graphene is semi-metallic while semiconducting carbon nanotubes usually exhibit p-type conductivity. To reduce the probability of getting false positive and false negative diagnosis, it is desirable to have complementary sensing capability by using both p-type and n-type semiconductors [23]. In_2O_3 is a well-known n-type semiconductor and has been successfully applied as the channel material for a variety of biosensors [24–29]. In our work, we fabricated In_2O_3 transistors using a lithography-free process. Our simplified fabrication method made In_2O_3 biosensors cost-efficient and suitable for large-scale COVID-19 clinical diagnosis.

FET-based biosensors can be combined with enzymatic reactions because many enzymatic reactions can release acidic or basic products, in which process the pH change of the environment will generate electronic signal of the FETs [30, 31]. Urease is the most common enzyme incorporated with FET-based biosensors [32–37]. However, urease displays poor stability [38–42], which would lose most of the enzymatic activity after being stored at 4 ℃ for 10 days [42]. In our work, we applied alkaline phosphatase as the enzyme reporter for our electronic biosensors. During the sensing process, alkaline phosphatase produces proton by enzymatically removing a phosphate group from the substrate compound, and the decreased pH value of the medium will then lead to an increase in the current of our In_2O_3 FETs. Phosphatase is widely used as the enzyme in commercial colorimetric ELISA kits (LoD: 16 pg/mL [43], 0.55 mg/mL [44]). Compared to urease, phosphatase is much more stable and suitable for long-term storage while maintaining high activity. Consequently, our biosensing platform with phosphatase overcomes the limit of electronic biosensing technique, whose application used to be constrained by the poor stability of enzyme reporter. Our biosensors display a prolonged shelf life and is advantageous for practical COVID-19 diagnosis.

In this work, Our In_2O_3 biosensors were able to detect S1 antigen of SARS-CoV-2 in both phosphate-buffered saline (PBS) buffer and universal transport medium (UTM) with a reliable performance and similar LoD of 100 fg/mL. Besides antigen detection, S1 protein IgG antibody detection in both PBS and human whole blood (WB) were also carried out. The detection performance in both mediums displayed LoD of 1 pg/mL. The similar detection results in different mediums indicate the capability of our electronic biosensors to eliminate the interference of salts, cells, and other particles in detected specimens. Taken together, our biosensors are highly sensitive and scalable, showing good potential for clinical SARS-CoV-2 diagnosis. Our findings shed light on a new generation of biosensors for rapid and highly sensitive COVID-19 screening, getting us closer to winning the fight against COVID-19 pandemic.

2 Results and discussion

2.1 Biosensors based on In_2O_3 nanoribbon FET devices

Figure 1(b) shows the photograph of the In_2O_3 nanoribbon FET devices on a Si/SiO_2 (500 nm) substrate. The lithography-free fabrication of the FETs includes two steps. First, In_2O_3 nanoribbons were defined by the first shadow mask and deposited using radio frequency (RF) sputtering technique. The channel length and width of the In_2O_3 nanoribbons were 500 and 25 μm, respectively (Fig. 1(c)), and the thickness was 18 nm (Fig. 1(d)). Next, the source and drain electrodes were defined by the second shadow mask. After alignment of the second mask, 1 nm Ti and 50 nm Au were deposited by electron beam evaporation. Twenty-eight biosensing chips can be fabricated on a 3-inch substrate, and each chip contains an array of 4 separate In_2O_3 FET devices.

The electrical performance of the devices was first characterized in ambient environment using an Agilent Semiconductor Analyzer 1500B. Nine different In_2O_3 FET devices were randomly picked over the substrate (labelled in Fig. 1(b)), and their drain current–back gate voltage (I_{DS}–V_{GS}) curves with the drain voltage fixed at 1 V are shown in Fig. 1(e). To further demonstrate the uniformity of our devices, I_{DS}–V_{GS} curves were measured for more devices at different locations on our substrate with drain voltage fixed at 150 mV and 5 V (Figs. S2(a) and S2(b) in the ESM), both of which show that our devices are uniform. Moreover, to demonstrate the stability of our devices, we have measured I_{DS}–V_{GS} curves of a single device for 20 times over a period of 1 week, as shown in (Fig. S2(c) in the ESM), which showed very little variation. Based on these measurements, we can deduce that our fabricated devices exhibit high uniformity and stability.

The I_{DS}–V_{GS} curves of the FET devices illustrate n-type transistor behavior with an average mobility of 108±4.3 $cm^2/V{\cdot}s$ (Fig. S3 in the ESM) and on-off ratio of ~1×10^5. Owing to the thick SiO_2 dielectric, the devices can be turned on only at high back gate voltage. Figure 1(e) demonstrates the electrical uniformity of In_2O_3 nanoribbon devices over the entire wafer.

Figure 1(f) shows the schematic diagram depicting the functionalization of our In_2O_3 devices for detection of S1 protein. The photograph of the experimental set up is shown in Fig. S1 in the ESM, a Teflon cell with an opening at the bottom was used to contain the medium in contact with the In_2O_3 biosensors. Prior to the electronic biosensing process, the In_2O_3 devices were first immersed in boiling acetone and isopropyl alcohol for 5 min each to clean the surface, followed by an O_2 plasma treatment to generate hydroxyl groups on the surface of In_2O_3. 3-Phosphonopropioninc acid, as the linker molecules, was then applied to bind with the hydroxyl groups on the surface. Subsequently, devices were functionalized with N-(3-dimethylaminopropyl)-N′-ethylcarbodiimide hydrochloride/N-hydroxysuccinimide (EDC/NHS), creating activated carboxyl groups to bind with amino groups from proteins. Next, capture antibodies that can specifically target S1 antigens of SARS-CoV-2 were applied and immobilized via reaction with the EDC/NHS groups on the surface. This immobilization process is followed by a washing step to rinse off unbounded antibodies as well as a blocking step by 10% bovine serum albumin (BSA) solution to deactivate the surface of In_2O_3 in order to avoid non-specific binding during consecutive processes. Target biomarkers were then introduced to our biosensors. As shown in Figure 1(f), S1 antigen solutions with known concentrations were dissolved in either PBS or UTM followed by a 1-hour incubation period. Next, biotinylated secondary antibody were introduced and incubated for 1 hour followed by a 40-min incubation of streptavidin conjugated phosphatase. Finally, phosphatase substrate solution was applied and an amperometric signal was recorded as the result of the detection. The total time required since applying biomarkers until obtaining final sensing result is nearly 3 hours, with actual detection time ranges between 10 to 15 min.

2.2 Electronic biosensing realized by enzymatic reaction of phosphatase

Our electronic detection of SARS-CoV-2 is based on enzymatic reaction of alkaline phosphatase. As shown in Fig. 2(a), when catalytic alkaline phosphatase is present, the phosphate group of the substrate compound would get removed during the reaction and protons would get produced, leading to a change in the solution's pH value. To prepare the substrate solution, 10 mg of 4-Nitrophenyl phosphate disodium salt hexahydrate, which is the commercial phosphatase substrate for colorimetric ELISA, was dissolved in 10 mL of 0.5 M $MgCl_2$ solution. The pH value of the substrate solution was then adjusted to 9.7 by NaOH solution. We monitored the pH change after manually mixing 5 μL of 1.5 mg/mL alkaline phosphatase solution with 3 mL of the substrate solution, and the pH value decreased by 1.3 in 5 minutes (Fig. 2(b)).

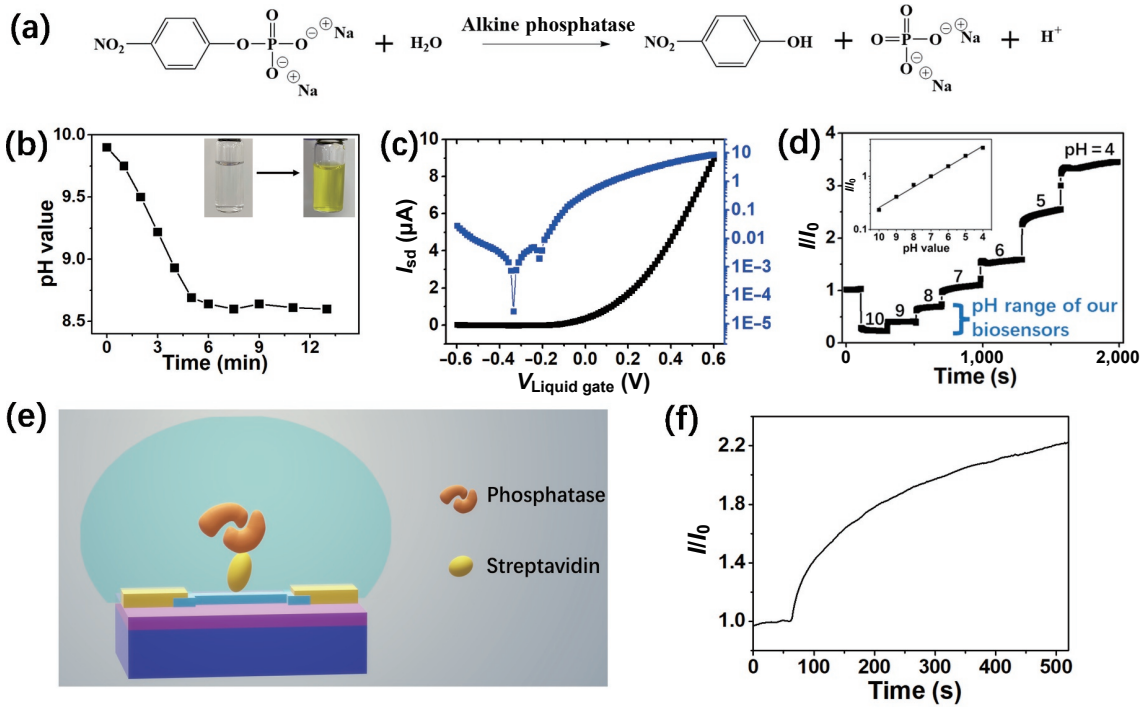

Figure 2 Mechanism of the electronic ELSIA. (a) Chemical equation of the enzymatic reaction catalyzed by phosphatase. (b) Change in pH value after mixing phosphatase with the substrate solution. The inset shows the simultaneous color change. (c) Drain current versus liquid gate voltage with drain voltage fixed at 1 V, plotted in linear and logarithmic scale. (d) Real-time responses obtained from an In_2O_3 nanoribbon device exposed to commercial buffer solutions with pH from 10 to 4. (e) Schematic illustration of the electronic biosensing setup for positive control, which demonstrates phosphatase is compatible with the electronic biosensing technique. (f) Real-time responses monitored from the positive control setup.

Our In_2O_3 nanoribbon FET devices served as a pH sensor in response to the pH change caused by the phosphatase enzymatic reaction. Hence, devices are required to operate in a wet environment (Fig. 1(f)). An Ag/AgCl reference electrode was used to apply liquid gate bias. Figure 2(c) shows the drain current–liquid gate voltage (I_{DS}–V_{GS}) curve of the devices immersed in 0.01×PBS buffer with the drain voltage fixed at 200 mV. Figure S4 in the ESM shows the family curves of drain current–drain voltage (I_{DS}–V_{DS}) where In_2O_3-FETs display good current saturation at high V_{DS}. Based on these measurements, we can deduce that our In_2O_3-FETs can be reliably and efficiently controlled using the liquid gate with phosphatase was directly attached to the FET device by EDC/NHS chemistry, while the detailed incubation process was similar to the S1 antigen detection described above.

To ensure the detection of the final amperometric signal, prior to adding substrate solution, the channel region of the In_2O_3 FET was immersed in $MgCl_2$ and NaOH solution with the on/off ratios (I_{on}/I_{off}) of 10^4.

When the enzymatic reaction starts, the deprotonated hydroxyl groups on the surface of In_2O_3 nanoribbons become protonated as the pH decreases. Therefore, the negative charges on the surface of In_2O_3 nanoribbons decrease and the conduction of the material increases. Figure 2(d) shows the current change of the FET devices in response to pH change, with a fixed liquid gate voltage at 150 mV and a fixed drain voltage at 200 mV, and the I_{DS} of the device increased by a factor of 14 as the pH changed from 10 to 4.

In order to demonstrate that In_2O_3 nanoribbon FET devices and phosphatase enzymatic reaction can be integrated for electronic biosensing, we performed a positive control experiment. Figure 2(e) depicts the schematic diagram of the sequence of molecule binding. The streptavidin-conjugated same pH value as the substrate solution. A liquid gate voltage of 150 mV was applied while the drain voltage was fixed at 200 mV to generate the observed baseline. Substrate solution was then added to trigger the enzymatic reaction and I_{DS} of the device was recorded as a function of time. As shown in Fig. 2(f), the I_{DS} started to increase as soon as the substrate was introduced with a current enhancement of 110% after 8 minutes.

Furthermore, to examine the interference in our biosensing results caused by potential electrochemical reaction happening in the substrate solution and the change in solution volume during the electrical measurement, we performed a negative control experiment. With fixed liquid gate voltage at 150 mV and the substrate solution (pH = 9.7), which is used in our biosensing setup, we measured I_{DS} over time, as shown in Fig. S5 in the ESM. We observed a very stable I_{DS} vs. time curve, indicating that no electrochemical reaction that can cause observable current change occurred within the rather small bias of 150 mV we used. In addition, we varied the volume of the substrate solution from 200 to 400 μL during this process and no current change was observed. Consequently, we can deduce that the volume change of the substrate solution does not affect the result of our biosensors.

2.3 Detection of SARS-CoV-2 spike protein in PBS and UTM

We performed electronic biosensing targeting at S1 antigen of SARS-CoV-2 spike protein in 1 × PBS with known concentrations ranging from 100 fg/mL to 1 ng/mL. Figure 3(a) shows the normalized responses for each concentration. After taking the average of sensing results from 5 different biosensors and subtracting the negative control, we obtained responses of 5%, 11%, 28%, 54% and 78% of current increase for antigen concentrations of 100 fg/mL, 1 pg/mL, 10 pg/mL, 100 pg/mL and 1 ng/mL S1, respectively (Fig. 3(c)). The negative control was performed by merely replacing the antigen biomarker with BSA solution during the functionalization process. The slight increase in the signal of the negative control can be caused by the non-specific binding of the phosphatase to the In_2O_3 nanoribbons.

The detection of S1 protein dissolved in UTM with the same range of concentrations was carried out as well. Universal transport medium is a common solvent for collection, transport, maintenance, and long-term freeze storage of clinical specimens containing viruses. It's widely used for cell culture, rapid antigen detection, PCR, and nucleic acid amplification assays. Hence, antigen detection in UTM helps to assess our biosensor to be used for clinical diagnosis of SARS-CoV-2. In order to simulate a real clinical setting, we have adopted a nasopharyngeal swab sample taken from a healthy person in our UTM-based detection setup. The swab was suspended in the UTM along with S1 protein. Figure 3(b) shows the obtained sensing signal. 4%, 10%, 25%, 53%, and 78% of current changes (average of 5 trials) have been

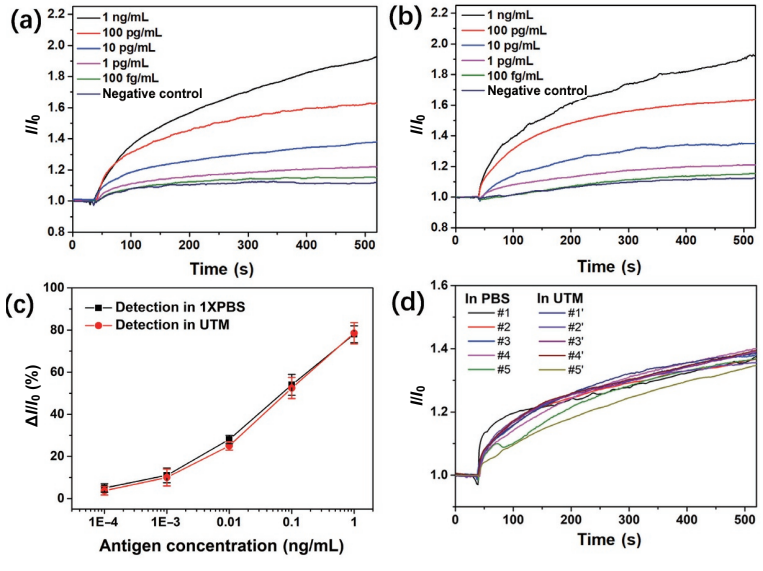

Figure 3 Detection of SARS-CoV-2 spike protein. (a) Real-time responses monitored at 100 fg/mL, 1 pg/mL, 10 pg/mL, 100 pg/mL and 1 ng/mL of S1 proteins in PBS. (b) Real-time responses monitored at 100 fg/mL, 1 pg/mL, 10 pg/mL, 100 pg/mL and 1 ng/mL of S1 proteins in UTM. (c) Plot of normalized responses at each S1 protein concentration, in nanograms per milliliter, n = 5, error bars represent standard deviation. (d) Real-time responses monitored using ten biosensors from four batches of fabrication at 10 pg/mL of S1 protein, showing the reproducibility of our technique.

generated in response to antigen concentrations of 100 fg/mL, 1 pg/mL, 10 pg/mL, 100 pg/mL and 1 ng/mL, respectively (Fig. 3(c)). The results of detections in PBS (black squares) and UTM (red dots) are plotted in Fig. 3(c). The results illustrated that the ingredients of UTM, such as Hank's balanced salts, BSA and sucrose, would not interfere with the sensing results. This finding reveals that our electronic biosensing approach can circumvent Debye screening from salts in the fluid, indicating that our biosensors can be used for clinical diagnostic testing without any special sample preparation or pretreatment.

The LoD of our biosensor reached 100 fg/mL, which is 2 orders of magnitude lower than conventional colorimetric ELISA [43, 44]. This could be caused by the local reaction nature of our sensing technique. We expected the local pH changes of the solution surrounding the In_2O_3 nanoribbon to generate the amperometric signal instead of changing the pH of the entire solution, which would require greater number of phosphatase molecules anchored to the surface of In_2O_3 and take a prolonged period of time for detection. This hypothesis can be supported by the measurement shown in Fig. S6 in the ESM, as bubbling the solution extensively to mix it thoroughly, the current dropped back to a point close to the baseline, indicating the pH of the entire solution didn't change much. Once the bubbling was stopped, the current increased again as the enzymatic reaction changed the local pH of the solution.

To investigate the reproducibility of our detection, we performed biosensing of 10 pg/mL S1 antigen in different mediums using devices from 4 different batches of fabrication. As shown in Fig. 3(d), 5 rounds of detection in PBS and 5 rounds of detection in UTM generated similar sensing responses. Hence, it is safe to say that our fabricated biosensors exhibit a remarkable reproducibility for large scale clinical diagnostic testing.

2.4 Detection of spike protein IgG antibody in PBS and human whole blood

To demonstrate the versatility of our electronic biosensing platform, we applied our In_2O_3 devices to detect SARS-CoV-2 spike protein IgG antibody. Figure 4(a) shows schematics of the structure of surfaced functionalized In_2O_3 nanoribbon for S1 protein specific antibody detection. In this structure, the sequence of molecule binding along with the conjugated antibody and S1 protein serve as the capturing component. After forming this capturing component, target antibody was incubated for 1 h. Biotin conjugated anti-Human IgG antibody was then introduced as the secondary antibody, and then streptavidin-conjugated phosphatase was introduced. Streptavidin would bind to biotin, and thus phosphatase got anchored to our biosensor surface, and the device became ready for electronic biosensing. Finally, amperometric signal was recorded while the device is immersed in liquid gate setup.

Figure 4(b) shows the amperometric signals generated as the result of detecting antibodies dissolved in PBS buffer solution. 1, 10, 100 pg/mL and 1 ng/mL concentrations of antibodies generated 18%, 37%, 65%, and 82% of current enhancement (average of 5 trials), respectively (Fig. 4(d)). It's worth noting that the anti-Human IgG antibody could potentially bind with the primary antibody. Therefore, to investigate the effect of this undesired binding, we performed a negative control experiment, where BSA solution was used to replace the target antibody. Figure 4(b) shows the result of this negative control (green curve) where a 4% current increase was generated. This indicates that the anti-Human IgG antibody could hardly bind with the primary antibody, which is already anchored to the surface of In_2O_3, and hence, would not affect the sensing results.

Furthermore, our biosensors exhibit high selectivity when detecting S1 protein specific antibody in physiological solutions, as demonstrated in Fig. 4(c). Here, we spiked target antibodies with known concentrations into human whole blood (WB) and carried out the detection. We varied S1 protein specific antibody concentration to include 1, 10, 100 pg/mL and 1 ng/mL, which led to current enhancement (average of 5 trials) of 16%, 29%, 58% and 77%, respectively (Fig. 4(d)). The results of the detection in PBS (black squares) and human whole blood (red dots) are plotted in Fig. 4(d). As depicted in the figure, antibodies spiked in PBS and WB generated analogous responses while the magnitude of sensing responses detecting antibody in blood is slightly lower than that in PBS. These miniscule differences could stem from the high viscosity of the whole blood, where precipitated blood cells can attach to the surface of the biosensor during the incubation period, and thus could induce interference with the sensing

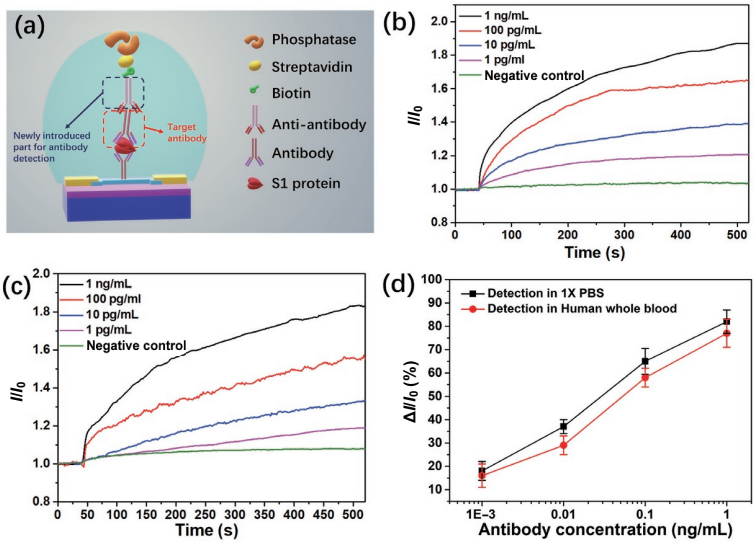

Figure 4 Detection of SARS-CoV-2 spike protein IgG antibody. (a) Schematic illustration of the electronic biosensing setup for antibody detection. Compared to Fig. 1(f), we have added anti-human IgG antibody (in blue dash box) so that the sensor can detect the IgG antibody of SARS-CoV-2 spike protein. (b) Real-time responses monitored at 1 pg/mL, 10 pg/mL, 100 pg/mL and 1 ng/mL of antibody in PBS. (c) Real-time responses monitored at 1 pg/mL, 10 pg/mL, 100 pg/mL and 1 ng/mL of antibody in human whole blood. (d) Plot of normalized responses at each antibody concentration, in nanograms per milliliter, n = 5, error bars represent standard deviation.

results. Nevertheless, we can safely say that the sensing behaviors in both mediums are mainly attributed to the binding of the target antibody.

The results of detecting SARS-CoV-2 S1 antigen in PBS and UTM, and S1 protein specific antibody in PBS and human whole blood reveal that our In_2O_3 devices and electronic biosensing approach can be highly sensitive, dual-functional biosensors for COVID-19 diagnosis. The ability of our biosensors to switch from antigen detection to antibody detection by simply adding an additional step of antigen incubation and changing the secondary antibody, along with their high immunity to interference caused by ions, cells, and other particles from complex fluids, makes our cost-efficient biosensors desirable for worldwide rapid screening of SARS-COV-2 virus with high sensitivity.

The demonstrated electronic biosensing platform based on phosphatase and shadow mask fabrication process is not limited to In_2O_3 material and SARS-CoV-2 biosensing. This technology has the potential to be applied to other semiconducting materials such as silicon nanowires [16, 45], metal oxide nanowires/nanoribbons [46], carbon nanotubes [47], graphene [48], and other two-dimensional materials [49] for biosensing applications. In addition, the electronic biosensing technique based on phosphatase has the potential to be generalized as a standard protocol of electronic biosensors for highly sensitive detection of various proteins with prolonged shelf life.

Since the enzyme and other reagents used in the functionalization of our biosensors are also used for commercial colorimetric ELISA kits, it is possible to integrate our biosensors with conventional colorimetric ELISA for a dual-readout biosensor platform. Such integration would improve the sensing characteristics with high reliability. In this platform, colorimetric signal can be used for quick and preliminary detection, while the electrical signal can subsequently be used for a more sensitive diagnosis.

3 Conclusions

We have demonstrated sensitive, scalable, and cost-efficient COVID-19 biosensors using electronic biosensing platform based on In_2O_3 FET devices functionalized with phosphatase. The devices were fabricated by a simple and cheap shadow mask method. Our biosensors were able to detect SARS-CoV-2 spike protein in UTM (LoD: 100 fg/mL) and S1 protein specific IgG antibody in human whole blood (LoD: 1 pg/mL), indicating its potential for clinical diagnostic testing. Our results can be instrumental for the management and control of the current pandemic and can possibly prevent further community transfer through early, rapid, and cost-efficient screening of COVID-19, giving us the upper hand to win the fight against this pandemic.

Acknowledgements

We would like to acknowledge the financial support of this research by King Abdul-Aziz City for Science and Technology (KACST) through The Center of Excellence for Nanotechnologies (CEGN).

Electronic Supplementary Material: Supplementary material (materials and methods for device fabrication, functionalization of In_2O_3 devices, photographs of the liquid gate measurement setup, mobilities of the nine devices labeled in Fig. 1(b), family curves of I_{DS}–V_{DS} with the liquid gate setup and current change after bubbling the substrate solution (current vs. time curve for S1 antigen detection)) is available in the online version of this article at https://doi.org/10.1007/10.1007/s12274-022-4190-0.

References

[1] WHO. *WHO Coronavirus Disease (COVID-19) Dashboard* [Online]. https://covid19.who.int/ (accessed Nov 1, 2021).

[2] WHO. *Guidance for Surveillance of SARS-CoV-2 Variants*: *Interim Guidance*, *9 August 2021* [Online]. https://www.who.int/publications/i/item/WHO_2019-nCoV_surveillance_variants (accessed Nov 1, 2021).

[3] WHO. *Weekly Epidemiological Update on COVID-19-10 August 2021* [Online]. https://www.who.int/publications/m/item/weekly-epidemiological-update-on-covid-19---10-august-2021 (accessed Nov 1, 2021).

[4] Goodell, J. W. COVID-19 and finance: Agendas for future research. *Finance Res. Lett.* **2020**, *35*, 101512.

[5] Chen, N. S.; Zhou, M.; Dong, X.; Qu, J. M.; Gong, F. Y.; Han, Y.; Qiu, Y.; Wang, J. L.; Liu, Y.; Wei, Y. et al. Epidemiological and clinical characteristics of 99 cases of 2019 novel coronavirus pneumonia in Wuhan, China: A descriptive study. *Lancet* **2020**, *395*, 507–513.

[6] Wang, D. W.; Hu, B.; Hu, C.; Zhu, F. F.; Liu, X.; Zhang, J.; Wang, B. B.; Xiang, H.; Cheng, Z. S.; Xiong, Y. et al. Clinical characteristics of 138 hospitalized patients with 2019 novel coronavirus-infected pneumonia in Wuhan, China. *JAMA* **2020**, *323*, 1061–1069.

[7] Zhu, N.; Zhang, D. Y.; Wang, W. L.; Li, X. W.; Yang, B.; Song, J. D.; Zhao, X.; Huang, B. Y.; Shi, W. F.; Lu, R. J. et al. A novel coronavirus from patients with pneumonia in China, 2019. *N. Engl. J. Med.* **2020**, *382*, 727–733.

[8] Lu, R. J.; Zhao, X.; Li, J.; Niu, P. H.; Yang, B.; Wu, H. L.; Wang, W. L.; Song, H.; Huang, B. Y.; Zhu, N. et al. Genomic characterisation and epidemiology of 2019 novel coronavirus: Implications for virus origins and receptor binding. *Lancet* **2020**, *395*, 565–574.

[9] Bastos, M. L.; Tavaziva, G.; Abidi, S. K.; Campbell, J. R.; Haraoui, L. P.; Johnston, J. C.; Lan, Z. Y.; Law, S.; MacLean, E.; Trajman, A. et al. Diagnostic accuracy of serological tests for Covid-19: Systematic review and meta-analysis. *BMJ* **2020**, *370*, m2516.

[10] Weissleder, R.; Lee, H.; Ko, J.; Pittet, M. J. COVID-19 diagnostics in context. *Sci. Transl. Med.* **2020**, *12*, eabc1931.

[11] Liu, G. Q.; Rusling J. F. COVID-19 antibody tests and their limitations. *ACS Sens.* **2021**, *6*, 593–612.

[12] World Health Organization. Laboratory testing for coronavirus disease (COVID-19) in suspected human cases: Interim guidance, 19 March 2020. Geneva: World Health Organization, 2020.

[13] Noh, J. Y.; Yoon, S. W.; Kim, D. J.; Lee, M. S.; Kim, J. H.; Na, W.; Song, D.; Jeong, D. G.; Kim, H. K. Simultaneous detection of severe acute respiratory syndrome, Middle East respiratory syndrome, and related bat coronaviruses by real-time reverse transcription PCR. *Arch. Virol.* **2017**, *162*, 1617–1623.

[14] Chan, J. F. W.; Yip, C. C. Y.; To, K. K. W.; Tang, T. H. C.; Wong, S. C. Y.; Leung, K. H.; Fung, A. Y. F.; Ng, A. C. K.; Zou, Z. J.; Tsoi, H. W. et al. Improved molecular diagnosis of COVID-19 by the novel, highly sensitive and specific COVID-19-RdRp/Hel real-time reverse transcription-PCR assay validated *in vitro* and with clinical specimens. *J. Clin. Microbiol.* **2020**, *58*, e00310–20.

[15] Fathi-Hafshejani, P.; Azam, N.; Wang, L.; Kuroda, M.A.; Hamilton M.C.; Hasim, S.; Mahjouri-Samani, M. Two-dimensional-material-based field-effect transistor biosensor for detecting COVID-19 virus (SARS-CoV-2). *ACS Nano* **2021**, *15(7)*, 11461–11469.

[16] Stern, E.; Klemic, J. F.; Routenberg, D. A.; Wyrembak, P. N.; Turner-Evans, D. B.; Hamilton, A. D.; LaVan, D. A.; Fahmy, T. M.; Reed, M. A. Label-free immunodetection with CMOS-compatible semiconducting nanowires. *Nature* **2007**, *445*, 519–522.

[17] Ishikawa, F. N.; Chang, H. K.; Curreli, M.; Liao, H. I.; Olson, C. A.; Chen, P. C.; Zhang, R.; Roberts, R. W.; Sun, R.; Cote, R. J. et al. Label-free, electrical detection of the SARS virus N-protein with nanowire biosensors utilizing antibody mimics as capture probes. *ACS Nano* **2009**, *3*, 1219–1224.

[18] Wang, B.; Zhao, C.; Wang, Z.; Yang, K. A.; Cheng, X.; Liu, W.; Yu, W.; Lin, S.; Zhao, Y.; Cheung, K. M. et al. Wearable aptamer-field-effect transistor sensing system for noninvasive cortisol monitoring. *Sci. Adv.* **2022**, *8(1)*, eabk0967.

[19] Chen, Y. T.; Ren, R.; Pu, H. H.; Guo, X. R.; Chang, J. B.; Zhou, G. H.; Mao, S.; Kron, M.; Chen, J. H. Field-effect transistor biosensor for rapid detection of Ebola antigen. *Sci. Rep.* **2017**, *7*, 10974.

[20] Afsahi, S.; Lerner, M. B.; Goldstein, J. M.; Lee, J.; Tang, X. L.; Bagarozzi, D. A. Jr.; Pan, D.; Locascio, L.; Walker, A.; Barron, F. et al. Novel graphene-based biosensor for early detection of Zika virus infection. *Biosens. Bioelectron.* **2018**, *100*, 85–88.

[21] Seo, G.; Lee, G.; Kim, M. J.; Baek, S. H.; Choi, M.; Ku, K. B.; Lee, C. S.; Jun, S.; Park, D.; Kim, H. G. et al. Rapid detection of COVID-19 causative virus (SARS-CoV-2) in human nasopharyngeal swab specimens using field-effect transistor-based biosensor. *ACS Nano* **2020**, *14*, 5135–5142.

[22] Shao, W. T.; Shurin, M. R.; Wheeler, S. E.; He, X. Y.; Star, A. Rapid detection of SARS-CoV-2 antigens using high-purity semiconducting single-walled carbon nanotube-based field-effect transistors. *ACS Appl. Mater. Interfaces* **2021**, *13*, 10321–10327.

[23] Li, C.; Curreli, M.; Lin, H.; Lei, B.; Ishikawa, F. N.; Datar, R.; Cote, R. J.; Thompson, M. E.; Zhou, C. W. Complementary detection of prostate-specific antigen using In_2O_3 nanowires and carbon nanotubes. *J. Am. Chem. Soc.* **2005**, *127*, 12484–12485.

[24] Kim, J.; Rim, Y. S.; Chen, H.; Cao, H. H.; Nakatsuka, N.; Hinton, H. L.; Zhao, C. Z.; Andrews, A. M.; Yang, Y.; Weiss, P. S. Fabrication of high-performance ultrathin In_2O_3 film field-effect transistors and biosensors using chemical lift-off lithography. *ACS Nano* **2015**, *9*, 4572–4582.

[25] Liu, Q. Z.; Liu, Y. H.; Wu, F. Q.; Cao, X.; Li, Z.; Alharbi, M.; Abbas, A. N.; Amer, M. R.; Zhou, C. W. Highly sensitive and wearable In_2O_3 nanoribbon transistor biosensors with integrated on-chip gate for glucose monitoring in body fluids. *ACS Nano* **2018**, *12*, 1170–1178.

[26] Chang, H. K.; Ishikawa, F. N.; Zhang, R.; Datar, R.; Cote, R. J.; Thompson, M. E.; Zhou, C. W. Rapid, label-free, electrical whole blood bioassay based on nanobiosensor systems. *ACS Nano* **2011**, *5*, 9883–9891.

[27] Zhao, C. Z.; Liu, Q. Z.; Cheung, K. M.; Liu, W. F.; Yang, Q.; Xu, X. B.; Man, T. X.; Weiss, P. S.; Zhou, C. W.; Andrews, A. M. Narrower nanoribbon biosensors fabricated by chemical lift-off lithography show higher sensitivity. *ACS Nano* **2021**, *15*, 904–915.

[28] Liu, Q. Z.; Zhao, C. Z.; Chen, M. R.; Liu, Y. H.; Zhao, Z. Y.; Wu, F. Q.; Li, Z.; Weiss, P. S.; Andrews, A. M.; Zhou, C. W. Flexible multiplexed In_2O_3 nanoribbon aptamer-field-effect transistors for biosensing. *iScience* **2020**, *23*, 101469.

[29] Nakatsuka, N.; Yang, K. A.; Abendroth, J. M.; Cheung, K. M.; Xu, X. B.; Yang, H. Y.; Zhao, C. Z.; Zhu, B. W.; Rim, Y. S.; Yang, Y. et al. Aptamer-field-effect transistors overcome Debye length limitations for small-molecule sensing. *Science* **2018**, *362*, 319–324.

[30] Schomburg, I.; Chang, A.; Placzek, S.; Söhngen, C.; Rother, M.; Lang, M.; Munaretto, C.; Ulas, S.; Stelzer, M.; Grote, A. et al. BRENDA in 2013: Integrated reactions, kinetic data, enzyme function data, improved disease classification: New options and contents in BRENDA. *Nucleic Acids Res.* **2013**, *41*, D764–D772.

[31] Danielsson, B.; Lundström, I.; Mosbach, K.; Stiblert, L. On a new enzyme transducer combination: The enzyme transistor. *Anal. Lett.* **1979**, *12*, 1189–1199.

[32] Alegret, S.; Bartrolí, J.; Jiménez, C.; Martínez-Fàbregas, E.; Martorell, D.; Valdés-Perezgasga, F. ISFET-based urea biosensor. *Sens. Actuators B:Chem.* **1993**, *16*, 453–457.

[33] Boubriak, O. A.; Soldatkin, A. P.; Starodub, N. F.; Sandrovsky, A. K.; El'skaya, A. K. Determination of urea in blood serum by a urease biosensor based on an ion-sensitive field-effect transistor. *Sens. Actuators B:Chem.* **1995**, *27*, 429–431.

[34] Mu, L. Y.; Droujinine, I. A.; Rajan, N. K.; Sawtelle, S. D.; Reed M. A. Direct, rapid, and label-free detection of enzyme-substrate interactions in physiological buffers using CMOS-compatible nanoribbon sensors. *Nano Lett.* **2014**, *14*, 5315–5322.

[35] Pijanowska, D. G.; Torbicz, W. pH-ISFET based urea biosensor. *Sens. Actuators B:Chem.* **1997**, *44*, 370–376.

[36] Liu, Q. Z.; Aroonyadet, N.; Song, Y.; Wang, X. L.; Cao, X.; Liu, Y. H.; Cong, S.; Wu, F. Q.; Thompson, M. E.; Zhou, C. W. Highly sensitive and quick detection of acute myocardial infarction biomarkers using In_2O_3 nanoribbon biosensors fabricated using shadow masks. *ACS Nano* **2016**, *10*, 10117–10125.

[37] Aroonyadet, N.; Wang, X. L.; Song, Y.; Chen, H. T.; Cote, R. J.; Thompson, M. E.; Datar, R. H.; Zhou, C. W. Highly scalable, uniform, and sensitive biosensors based on top-down indium oxide nanoribbons and electronic enzyme-linked immunosorbent assay. *Nano Lett.* **2015**, *15*, 1943–1951.

[38] Nannipieri, P.; Ceccanti, B.; Cervelli, S.; Sequi, P. Stability and kinetic properties of humus-urease complexes. *Soil Biol. Biochem.* **1978**, *10*, 143–147.

[39] Poźniak, G.; Krajewska, B.; Trochimczuk, W. Urease immobilized on modified polysulphone membrane: Preparation and properties. *Biomaterials* **1995**, *16*, 129–134.

[40] Reddy, K. R. C.; Kayastha, A. M. Improved stability of urease upon coupling to alkylamine and arylamine glass and its analytical use. *J. Mol. Catal. B:Enzym.* **2006**, *38*, 104–112.

[41] Yang, Z. P.; Si, S. H.; Zhang, C. J. Study on the activity and stability of urease immobilized onto nanoporous alumina membranes. *Micropor. Mesopor. Mater.* **2008**, *111*, 359–366.

[42] Yang, D.; Fan, J. H.; Cao, F. Y.; Deng, Z. J.; Pojman, J. A.; Ji, L. Immobilization adjusted clock reaction in the urea-urease-H^+ reaction system. *RSC Adv.* **2019**, *9*, 3514–3519.

[43] Ko, Y. C.; Mukaida, N.; Panyutich, A.; Voitenok, N. N.; Matsushima, K.; Kawai, T.; Kasahara, T. A sensitive enzyme-linked immunosorbent assay for human interleukin-8. *J. Immunol. Methods* **1992**, *149*, 227–235.

[44] Daniilidou, M.; Tsolaki, M.; Giannakouros, T.; Nikolakaki, E. Detection of elevated antibodies against SR protein kinase 1 in the serum of Alzheimer's disease patients. *J. Neuroimmunol.* **2011**, *238*, 67–72.

[45] Cui, Y.; Wei, Q. Q.; Park, H.; Lieber, C. M. Nanowire nanosensors for highly sensitive and selective detection of biological and chemical species. *Science* **2001**, *293*, 1289–1292.

[46] Pan, Z. W.; Dai, Z. R.; Wang, Z. L. Nanobelts of semiconducting oxides. *Science* **2001**, *291*, 1947–1949.

[47] Chen, R. J.; Zhang, Y. G.; Wang, D. W.; Dai, H. J. Noncovalent sidewall functionalization of single-walled carbon nanotubes for protein immobilization. *J. Am. Chem. Soc.* **2001**, *123*, 3838–3839.

[48] Shao, Y. Y.; Wang, J.; Wu, H.; Liu, J.; Aksay, I. A.; Lin, Y. H. Graphene based electrochemical sensors and biosensors: A review. *Electroanalysis* **2010**, *22*, 1027–1036.

[49] Wang, Y. H.; Huang, K. J.; Wu, X. Recent advances in transition-metal dichalcogenides based electrochemical biosensors: A review. *Biosens. Bioelectron.* **2017**, *97*, 305–316.